

Fusion of Active and Passive Measurements for Robust and Scalable Positioning

Hong Zhu^{1,2}, Alexander Venus^{1,2}, Erik Leitinger^{1,2}, Stefan Tertinek³, and Klaus Witrisal^{1,2}

¹Graz University of Technology, Austria, ³NXP Semiconductors, Austria,

²Christian Doppler Laboratory for Location-aware Electronic Systems

Abstract—This paper addresses the challenge of achieving reliable and robust positioning of a mobile agent, such as a radio device carried by a person, in scenarios where direct line-of-sight (LOS) links are obstructed or unavailable. The human body is considered as an extended object that scatters, attenuates and blocks the radio signals. We propose a novel particle-based sum-product algorithm (SPA) that fuses active measurements between the agent and anchors with passive measurements from pairs of anchors reflected off the body. We first formulate radio signal models for both active and passive measurements. Then, a joint tracking algorithm that utilizes both active and passive measurements is developed for the extended object. The algorithm exploits the probabilistic data association (PDA) for multiple object-related measurements. The results demonstrate superior accuracy during and after the obstructed line-of-sight (OLOS) situation, outperforming conventional methods that solely rely on active measurements. The proposed joint estimation approach significantly enhances the localization robustness via radio sensing.

Index Terms—robust positioning, active and passive measurements, extended object tracking, data association

I. INTRODUCTION

In the realm of wireless communication and location-based services, radio localization stands as a paramount endeavor. Among the various technologies being explored, ultra wide band (UWB) radio is a particularly attractive option for radio sensing applications. UWB radio offers superior temporal resolution, enabling the observation of multipath components (MPCs) from the environment or scattering paths reflected from objects [1], [2]. Besides, UWB is a wireless communication technology that has been developed to supply localization and sensing in an optimal way. This opens up a wide range of possibilities for various functionalities and applications, particularly in the field of mobility and transportation [3]–[5]. Safety-critical applications, such as autonomous driving [6], medical services [7], and keyless access systems [8], greatly benefit from the capabilities offered by radio sensing and communications.

The human body has indispensable effect on the robustness of the positioning algorithms, as it can cause complete blockage of line-of-sight (LOS) path to anchors, as well as dispersive and attenuated effects in the radio signals [9]. The human body can be considered as an extended object. To

The financial support by the Christian Doppler Research Association, the Austrian Federal Ministry for Digital and Economic Affairs and the National Foundation for Research, Technology and Development is gratefully acknowledged.

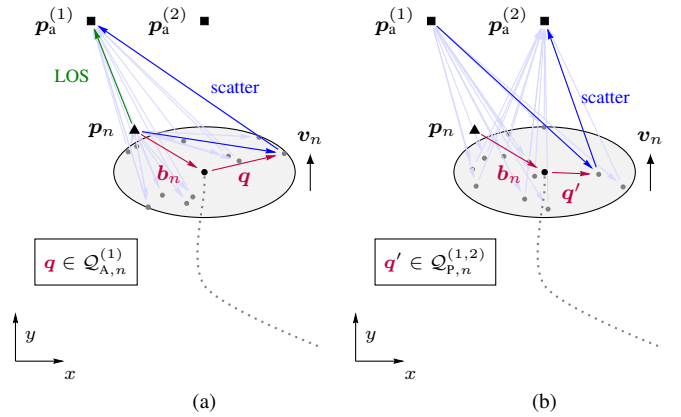


Fig. 1. Generic environment with a moving agent and two anchors at time n with exemplary signal propagation paths for (a) an active signal from the agent to anchor 1 and (b) a passive signal between anchor 1 and 2.

resolve problems related to extended object tracking (EOT), ellipses [10]–[14], rectangles [15], [16], and star convex shapes [17]–[19] can be used to model objects. The extended object can generate a diverse range of measurements from spatially dispersed reflection points. The challenging aspect of the EOT problem is fusing data from multiple object-related measurements at each time step [20]–[22]. Probabilistic data association (PDA) is a Bayesian method commonly applied in target tracking to handle measurement origin uncertainty [23], [24]. It can make use of the extracted measurement information, such as delays and amplitudes, to update the state estimate of the object in the presence of clutter [25], [26]. Recently, the sum-product algorithm (SPA) based on factor graphs has been investigated for the tracking of extended objects by exploiting probabilistic data association. Note that the proposed SPA has low computational complexity since it scales linearly in the number of measurements.

In this work, we consider both the measurements between the mobile agent and anchors, referred to as *active measurements*, as well as the measurements among anchors reflected off the human body, referred to as *passive measurements*. We first derive the UWB off-body radio signal models, describing the human body as an extended object. Additionally, based on a factor graph designed for joint active and passive estimation, we develop a particle-based SPA for robust sequential tracking of the extended object, fusing multiple object-related measurements originating from active and passive radar measurements.

II. RADIO SIGNAL MODEL

At each time step n , a mobile agent at position \mathbf{p}_n transmits a signal, and each anchor $j \in \{1, \dots, J\}$ at position $\mathbf{p}_a^{(j)} = [p_{ax}^{(j)} \ p_{ay}^{(j)}]^T$ acts as a receiver, capturing active measurements. Synchronously, pairs of anchors (j, j') exchange signals, capturing passive measurements from the human body. Note that the anchors act as receivers and transmitters. The human body is modeled as an extended object (EO) that is rigidly coupled to the mobile agent. The bias between the mobile agent and the body center is denoted as \mathbf{b}_n . An example is shown in Fig. 1. We refer to the mobile agent that is coupled with the extended object as the extended agent. For extended-object measurements, we assume the scatters are generated uniformly on the human body, and the human body is regarded as a scattering volume. We describe the scattering volume for active and passive measurements as $\mathbf{Q}_{A,n}^{(j)}$ and $\mathbf{Q}_{P,n}^{(j,j')}$ for received anchor j at time n , respectively. Each point-source scatter from the volume $\mathbf{Q}_{A,n}^{(j)}$ and $\mathbf{Q}_{P,n}^{(j,j')}$ is denoted by its position \mathbf{q} and \mathbf{q}' , respectively [27], [28].

A. Active Radio Signal

At each time step n , a radio signal is transmitted from the mobile agent and received at the j th anchor (see Fig. 1). The complex baseband signal received at j th anchor is modeled as

$$r_{A,n}^{(j)}(t) = \alpha_n^{(j)} s(t - \tau_n^{(j)}) + \sum_{\mathbf{q} \in \mathbf{Q}_{A,n}^{(j)}} \alpha_{\mathbf{q},n}^{(j)} \beta_{\mathbf{q}} s(t - \tau_{\mathbf{q},n}^{(j)}) + w_n^{(j)}(t) \quad (1)$$

where $\alpha_n^{(j)}$ and $\tau_n^{(j)}$ are the complex amplitude and delay of the LOS component from active measurements. The received signal of anchor j also consists of the scatter components originating from the scattering volume $\mathbf{Q}_{A,n}^{(j)}$. The complex amplitude and delay of the scatter component are denoted as $\alpha_{\mathbf{q},n}^{(j)}$ and $\tau_{\mathbf{q},n}^{(j)}$, and $\alpha_{\mathbf{q},n}^{(j)} = \alpha_A / \|(\mathbf{p}_n + \mathbf{b}_n + \mathbf{q}) - \mathbf{p}_a^{(j)}\|$, for $\mathbf{q} \in \mathbf{Q}_{A,n}^{(j)}$, with α_A describing the amplitude of the transmitted signal from the mobile agent, and $\beta_{\mathbf{q}}$ is the relative dampening variable for active measurements. The second term $w_n^{(j)}(t)$ accounts for measurement noise modeled as additive white Gaussian noise (AWGN) with double-sided power spectral density $N_0/2$. The propagation delay of the LOS path and scatter path¹ is given by

$$\tau_n^{(j)} = \|\mathbf{p}_n - \mathbf{p}_a^{(j)}\|/c \quad (2)$$

$$\tau_{\mathbf{q},n}^{(j)} = \|(\mathbf{p}_n + \mathbf{b}_n + \mathbf{q}) - \mathbf{p}_a^{(j)}\|/c \quad (3)$$

respectively, where $\mathbf{q} \in \mathbf{Q}_{A,n}^{(j)}$ and c is the speed of light.

B. Passive Radio Signal

At each time step n , a radio signal is transmitted from j' th anchor and received at j th anchor. The complex baseband signal received at j th anchor is modeled as

$$r_{P,n}^{(j,j')}(t) = \sum_{\mathbf{q}' \in \mathbf{Q}_{P,n}^{(j,j')}} \alpha_{\mathbf{q}',n}^{(j,j')} \beta_{\mathbf{q}'} s(t - \tau_{\mathbf{q}',n}^{(j,j')}) + w_n^{(j,j')}(t) \quad (4)$$

¹Note that here we ignore the distance from the mobile agent to scatter when we calculate the propagation delay of scatter component of active case.

where $\alpha_{\mathbf{q}',n}^{(j,j')}$ and $\tau_{\mathbf{q}',n}^{(j,j')}$ are the complex amplitude and delay of the scatter component in $\mathbf{Q}_{P,n}^{(j,j')}$, and $\alpha_{\mathbf{q}',n}^{(j,j')} = \alpha_P^{(j')}/(\|(\mathbf{p}_n + \mathbf{b}_n + \mathbf{q}') - \mathbf{p}_a^{(j')}\| \|(\mathbf{p}_n + \mathbf{b}_n + \mathbf{q}') - \mathbf{p}_a^{(j)}\|)$, for $\mathbf{q}' \in \mathbf{Q}_{P,n}^{(j,j')}$, with $\alpha_P^{(j')}$ describing the amplitude of the transmitted signal from anchor j' , and $\beta_{\mathbf{q}'}$ is the dampening variable for passive measurement. The propagation delay of the passive measurement is given by

$$\tau_{\mathbf{q}',n}^{(j,j')} = (\|(\mathbf{p}_n + \mathbf{b}_n + \mathbf{q}') - \mathbf{p}_a^{(j')}\| + \|(\mathbf{p}_n + \mathbf{b}_n + \mathbf{q}') - \mathbf{p}_a^{(j)}\|)/c \quad (5)$$

where $\mathbf{q}' \in \mathbf{Q}_{P,n}^{(j,j')}$.

C. Signal Parameter Estimation

At time n , measurements which are extracted from the active radio signal are called active measurements $\mathbf{z}_{A,n}$, while measurements which are extracted from the passive radio signal are called passive measurements $\mathbf{z}_{P,n}$. We define the vectors $\mathbf{z}_{A,n} = [\mathbf{z}_{A,n}^{(1)T} \dots \mathbf{z}_{A,n}^{(J)T}]^T$ and $\mathbf{z}_{P,n} = [\mathbf{z}_{P,n}^{(1,1)T} \dots \mathbf{z}_{P,n}^{(J,J)T}]^T$ for the measurement vectors per time n . For each received anchor j , we define $\mathbf{z}_{A,n}^{(j)} = [\mathbf{z}_{A,n,1}^{(j)}, \dots, \mathbf{z}_{A,n,M_{A,n}^{(j)}}^{(j)}]$, with $M_{A,n}^{(j)}$ being the number of active measurements. Each active measurement $\mathbf{z}_{A,n,l}^{(j)} = [z_{A,d,n,l}^{(j)} \ z_{A,u,n,l}^{(j)}]^T$, $l \in \{1, \dots, M_{A,n}^{(j)}\}$ contains a distance measurement $z_{A,d,n,l}^{(j)} \in [0, d_{\max}]$, where d_{\max} is the maximum measurement distance, and a normalized amplitude measurement $z_{A,u,n,l}^{(j)} \in [\gamma, \infty)$, where γ is the detection threshold. For the passive case, we define $\mathbf{z}_{P,n}^{(j,j')} = [\mathbf{z}_{P,n,1}^{(j,j')}, \dots, \mathbf{z}_{P,n,M_{P,n}^{(j,j')}}^{(j,j')}]$ with $M_{P,n}^{(j,j')}$ being the number of passive measurements. Each passive measurement $\mathbf{z}_{P,n,l}^{(j,j')} = [z_{P,d,n,l}^{(j,j')} \ z_{P,u,n,l}^{(j,j')}]^T$, $l \in \{1, \dots, M_{P,n}^{(j,j')}\}$ contains a distance measurement $z_{P,d,n,l}^{(j,j')} \in [0, d_{\max}]$ and a normalized amplitude measurement $z_{P,u,n,l}^{(j,j')} \in [\gamma, \infty)$.

III. JOINT ACTIVE AND PASSIVE TRACKING METHOD

In this section, we introduce a Bayesian factor graph-based SPA that fuses joint active and passive measurements. Since the human body is modeled as an extended object, the proposed algorithm is based on the multiple-measurement-to-object data association.

A. System Model

At time n , the extended agent state is described by a kinematic state and an extent state. The kinematic state $\mathbf{x}_n = [\mathbf{p}_n^T \ \mathbf{v}_n^T \ \mathbf{b}_n^T]^T$ consists of the mobile agent's position $\mathbf{p}_n = [p_{xn} \ p_{yn}]^T$, the velocity $\mathbf{v}_n = [v_{xn} \ v_{yn}]^T$, and the bias between the mobile agent and the body center $\mathbf{b}_n = [b_{xn} \ b_{yn}]^T$. The shape of the extended object is approximated by an ellipse. The extent state is modeled as $\mathbf{X}_n = \mathbf{A}_n \mathbf{E} \mathbf{A}_n^T$, while $\mathbf{E} \in \mathbb{R}^{2 \times 2}$ is a symmetric, positive semidefinite matrix that describes the 2-D ellipse². It is further assumed that

²At present, we assume the body shape is not changed over time, thus the extent state is an constant matrix varying with body rotation.

the square root of the eigenvalues of \mathbf{E} is proportional to the object's semi-axis [21], [29]. The rotation matrix $\mathbf{A}_n = [\cos(\theta_n), -\sin(\theta_n); \sin(\theta_n), \cos(\theta_n)]$ is formulated with θ_n describing the body orientation. The body orientation is determined from the velocity states as $\theta_n = \text{atan}(\frac{v_{yn}}{v_{xn}})$.

B. Measurement Model

1) *LOS Measurement Model*: The LOS likelihood function (LHF) of an individual active measurement is given by

$$f_{\text{LOS}}(\mathbf{z}_{A,n,l}^{(j)}|\mathbf{x}_n) = f_{\text{N}}(z_{A,d,n,l}^{(j)}; h_{\text{LOS}}(\mathbf{x}_n, \mathbf{p}_a^{(j)}), \sigma_d^2(z_{A,u,n,l}^{(j)})) \quad (6)$$

where $f_{\text{N}}(x; \mu, \sigma^2)$ is the Gaussian PDF, with mean $h_{\text{LOS}}(\mathbf{x}_n, \mathbf{p}_a^{(j)}) = \|\mathbf{p}_n - \mathbf{p}_a^{(j)}\|$ being the LOS measurement function and variance $\sigma_d^2(z_{A,u,n,l}^{(j)})$. The variance is determined from the Fisher information given by $\sigma_d^2(z_{A,u,n,l}^{(j)}) = c^2/(8\pi^2\beta_{\text{bw}}^2(z_{A,u,n,l}^{(j)}))^2$, where β_{bw} is the root mean squared bandwidth [30], [31].

2) *Scattering Measurement Model*: The scattering LHF of individual active and passive measurements are described as

$$f(\mathbf{z}_{A,n,l}^{(j)}|\mathbf{x}_n, \zeta_{A,n,l}^{(j)}) \triangleq f_{\text{N}}(z_{A,d,n,l}^{(j)}; h_{\text{A}}(\mathbf{x}_n, \zeta_{A,n,l}^{(j)}, \mathbf{p}_a^{(j)}), \sigma_d^2(z_{A,u,n,l}^{(j)})) \quad (7)$$

and

$$f(\mathbf{z}_{P,n,l}^{(j,j')}|\mathbf{x}_n, \zeta_{P,n,l}^{(j,j')}) \triangleq f_{\text{N}}(z_{P,d,n,l}^{(j,j')}; h_{\text{P}}(\mathbf{x}_n, \zeta_{P,n,l}^{(j,j')}, \mathbf{p}_a^{(j')}, \mathbf{p}_a^{(j)}), \sigma_d^2(z_{P,u,n,l}^{(j,j')})) \quad (8)$$

respectively, where $h_{\text{A}}(\mathbf{x}_n, \zeta_{A,n,l}^{(j)}, \mathbf{p}_a^{(j)}) = \|\mathbf{p}_n + \mathbf{b}_n + \zeta_{A,n,l}^{(j)} - \mathbf{p}_a^{(j)}\|$ and $h_{\text{P}}(\mathbf{x}_n, \zeta_{P,n,l}^{(j,j')}, \mathbf{p}_a^{(j')}, \mathbf{p}_a^{(j)}) = \|\mathbf{p}_n + \mathbf{b}_n + \zeta_{P,n,l}^{(j,j')} - \mathbf{p}_a^{(j')}\| + \|\mathbf{p}_n + \mathbf{b}_n + \zeta_{P,n,l}^{(j,j')} - \mathbf{p}_a^{(j)}\|$ are the nonlinear measurement functions of active scattering measurements and passive scattering measurements, respectively. Furthermore, we assume that $\zeta_{A,n,l}^{(j)}$ and $\zeta_{P,n,l}^{(j,j')}$ are the relative positions of scatters with respect to \mathbf{p}_n that generate $\mathbf{z}_{A,n,l}^{(j)}$ and $\mathbf{z}_{P,n,l}^{(j,j')}$. The extent state \mathbf{X}_n is used to define the covariance matrix of a Gaussian PDF³ that models the scattering distribution due to the geometric shape as $f(\zeta_{A,n,l}^{(j)}|\mathbf{X}_n) \triangleq f_{\text{N}}(\zeta_{A,n,l}^{(j)}; \mathbf{0}, \mathbf{X}_n)$ and $f(\zeta_{P,n,l}^{(j,j')}|\mathbf{X}_n) \triangleq f_{\text{N}}(\zeta_{P,n,l}^{(j,j')}; \mathbf{0}, \mathbf{X}_n)$.

The scattering measurement likelihood conditioned on \mathbf{x}_n and \mathbf{X}_n is a convolution of the noise distribution and the scattering distribution [21]. The LHF conditioned on \mathbf{x}_n and \mathbf{X}_n of an individual scattering measurement can be obtained by integrating out the scattering variables. Hence, the active scattering LHF can be obtained as

$$\begin{aligned} f_{\text{AS}}(\mathbf{z}_{A,n,l}^{(j)}|\mathbf{x}_n, \mathbf{X}_n) &= \int f(\mathbf{z}_{A,n,l}^{(j)}|\mathbf{x}_n, \zeta_{A,n,l}^{(j)})f(\zeta_{A,n,l}^{(j)}|\mathbf{X}_n)d\zeta_{A,n,l}^{(j)} \\ &= f_{\text{N}}(z_{A,d,n,l}^{(j)}; \bar{h}_{\text{A}}(\mathbf{x}_n, \mathbf{p}_a^{(j)}), \sigma_d^2(z_{A,u,n,l}^{(j)}) + l_{A,n}^{(j)}) \end{aligned} \quad (9)$$

³It is shown in [12] that for an elliptically shaped object the uniform distribution can be approximated by a Gaussian distribution.

where $\bar{h}_{\text{A}}(\mathbf{x}_n, \mathbf{p}_a^{(j)}) = \|\mathbf{p}_n + \mathbf{b}_n - \mathbf{p}_a^{(j)}\|$. We use the unscented transformation (UT) [32] for nonlinear transform of the scatter distribution $f(\zeta_{A,n,l}^{(j)}|\mathbf{X}_n)$ from position domain to delay domain. $l_{A,n}^{(j)}$ is the variance of the sigma points transformed by the nonlinear function $h_{\text{A}}(\cdot)$. The passive scattering LHF can be obtained as

$$\begin{aligned} f_{\text{PS}}(\mathbf{z}_{P,n,l}^{(j,j')}|\mathbf{x}_n, \mathbf{X}_n) &= \int f(\mathbf{z}_{P,n,l}^{(j,j')}|\mathbf{x}_n, \zeta_{P,n,l}^{(j,j')})f(\zeta_{P,n,l}^{(j,j')}|\mathbf{X}_n)d\zeta_{P,n,l}^{(j,j')} \\ &= f_{\text{N}}(z_{P,d,n,l}^{(j,j')}; \bar{h}_{\text{P}}(\mathbf{x}_n, \mathbf{p}_a^{(j')}, \mathbf{p}_a^{(j)}), \sigma_d^2(z_{P,u,n,l}^{(j,j')}) + l_{P,n}^{(j,j')}) \end{aligned} \quad (10)$$

where $\bar{h}_{\text{P}}(\mathbf{x}_n, \mathbf{p}_a^{(j')}, \mathbf{p}_a^{(j)}) = \|\mathbf{p}_n + \mathbf{b}_n - \mathbf{p}_a^{(j')}\| + \|\mathbf{p}_n + \mathbf{b}_n - \mathbf{p}_a^{(j)}\|$. Similar to the active case, $l_{P,n}^{(j,j')}$ is the variance of the sigma points transformed by the nonlinear function $h_{\text{P}}(\cdot)$.

3) *Active and Passive Measurement Model*: The active measurement model including the LOS path and the scattering paths is given as

$$\begin{aligned} f_{\text{A}}(\mathbf{z}_{A,n,l}^{(j)}|\mathbf{x}_n, \mathbf{X}_n) &= f_{\text{LOS}}(\mathbf{z}_{A,n,l}^{(j)}|\mathbf{x}_n) + f_{\text{AS}}(\mathbf{z}_{A,n,l}^{(j)}|\mathbf{x}_n, \mathbf{X}_n) \end{aligned} \quad (11)$$

and the passive measurement model including only the scattering paths is given as

$$f_{\text{P}}(\mathbf{z}_{P,n,l}^{(j,j')}|\mathbf{x}_n, \mathbf{X}_n) = f_{\text{PS}}(\mathbf{z}_{P,n,l}^{(j,j')}|\mathbf{x}_n, \mathbf{X}_n) \quad (12)$$

C. Data Association Uncertainty

For each anchor j , the measurements $\mathbf{z}_{A,n}^{(j)}$ and $\mathbf{z}_{P,n}^{(j,j')}$ are subject to data association uncertainty. It is not known which measurement is associated with the LOS path, which measurements originate from the extended object, or if a measurement did not originate from the LOS path and the object, i.e. clutter. The association variables $a_{A,n,l}^{(j)} \in \{0, 1\}$ and $a_{P,n,l}^{(j,j')} \in \{0, 1\}$ specify whether a single measurement is object-related, which is denoted by 1, or not, which is denoted by 0. Furthermore, let $\mathbf{a}_{A,n}^{(j)} = [a_{A,n,1}^{(j)}, \dots, a_{A,n,M_{A,n}^{(j)}}^{(j)}]$ and $\mathbf{a}_{P,n}^{(j,j')} = [a_{P,n,1}^{(j,j')}, \dots, a_{P,n,M_{P,n}^{(j,j')}}^{(j,j')}]$, as well as $\mathbf{a}_{A,n} = [a_{A,n}^{(1)\text{T}} \dots a_{A,n}^{(J)\text{T}}]^{\text{T}}$ and $\mathbf{a}_{P,n} = [a_{P,n}^{(1,1)\text{T}} \dots a_{P,n}^{(J,J)\text{T}}]^{\text{T}}$.

The number of object-related measurements is Poisson distributed with mean μ_m . The number of clutter measurement is also Poisson distributed with mean μ_c , and clutter measurements are independent and distributed according to the uniform distribution $f_c(\mathbf{z}_{A,n,l}^{(j)})$ and $f_c(\mathbf{z}_{P,n,l}^{(j,j')})$. Conditioned on \mathbf{x}_n and \mathbf{X}_n , the object-related measurements are independent of the other measurements. The pseudo-likelihood function for active and passive cases can be represented as [10]

$$\begin{aligned} g_{\text{A}}(\mathbf{z}_{A,n,l}^{(j)}|\mathbf{x}_n, \mathbf{X}_n, a_{A,n,l}^{(j)}) &= \begin{cases} \frac{\mu_m f_{\text{A}}(\mathbf{z}_{A,n,l}^{(j)}|\mathbf{x}_n, \mathbf{X}_n)}{\mu_c f_c(\mathbf{z}_{A,n,l}^{(j)})}, & a_{A,n,l}^{(j)} = 1 \\ 1, & a_{A,n,l}^{(j)} = 0 \end{cases} \end{aligned} \quad (13)$$

and

$$g_{\text{P}}(\mathbf{z}_{P,n,l}^{(j,j')}|\mathbf{x}_n, \mathbf{X}_n, a_{P,n,l}^{(j,j')})$$

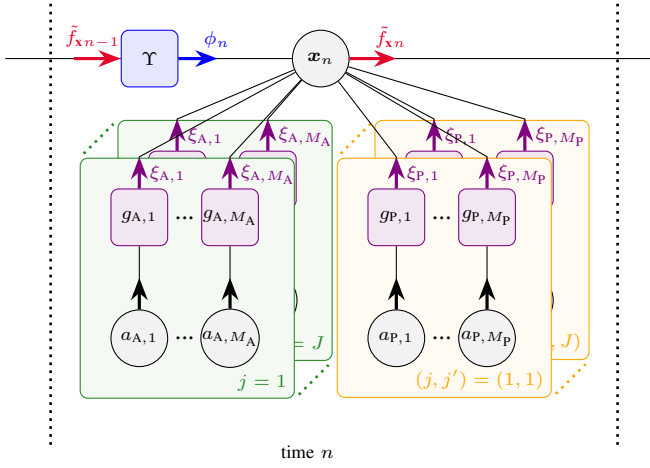


Fig. 2. Factor graph representing the factorization of the joint posterior PDF in (15) and the messages according to the SPA. For following short notations are used: $M_A \triangleq M_{A,n}^{(j)}$, $M_P \triangleq M_{P,n}^{(j)}$, $a_{A,l} \triangleq a_{A,n,l}^{(j)}$, $a_{P,l} \triangleq a_{P,n,l}^{(j,j')}$, $g_{A,l} \triangleq g_{A,n,l}^{(j)}$, $g_{P,l} \triangleq g_{P,n,l}^{(j,j')}$, $\xi_{A,l} \triangleq \xi_{A,n,l}^{(j)}$, $\xi_{P,l} \triangleq \xi_{P,n,l}^{(j,j')}$.

$$= \begin{cases} \frac{\mu_m f_P(z_{P,n,l}^{(j,j')} | \mathbf{x}_n, \mathbf{X}_n)}{\mu_c f_c(z_{P,n,l}^{(j,j')})}, & a_{P,n,l}^{(j,j')} = 1 \\ 1, & a_{P,n,l}^{(j,j')} = 0 \end{cases} \quad (14)$$

respectively.

D. Joint Posterior and Factor Graph

We model the evolution of \mathbf{x}_n over time n as an independent first-order Markov process, which is defined by the state transition PDF $f(\mathbf{x}_n | \mathbf{x}_{n-1})$. We assume that the measurements $\mathbf{z}_{A,n}$ and $\mathbf{z}_{P,n}$ are observed and thus fixed. Let $\mathbf{x} = [\mathbf{x}_1^T \cdots \mathbf{x}_n^T]^T$, $\mathbf{a}_A = [\mathbf{a}_{A,1}^T \cdots \mathbf{a}_{A,n}^T]^T$, $\mathbf{a}_P = [\mathbf{a}_{P,1}^T \cdots \mathbf{a}_{P,n}^T]^T$, $\mathbf{z}_A = [\mathbf{z}_{A,1}^T \cdots \mathbf{z}_{A,n}^T]^T$, and $\mathbf{z}_P = [\mathbf{z}_{P,1}^T \cdots \mathbf{z}_{P,n}^T]^T$. According to the Bayes's rule and other related independence assumptions [33], the joint posterior PDF of all estimated states for time n and all J anchors can be derived as

$$\begin{aligned} & f(\mathbf{x}, \mathbf{a}_A, \mathbf{a}_P | \mathbf{z}_A, \mathbf{z}_P) \\ & \propto f(\mathbf{x}_0) \prod_{n'=1}^n \Upsilon(\mathbf{x}_{n'} | \mathbf{x}_{n'-1}) \\ & \quad \times \prod_{j=1}^J \prod_{l=1}^{M_{A,n'}^{(j)}} g_A(z_{A,n',l}^{(j)} | \mathbf{x}_{n'}, \mathbf{X}_{n'}, a_{A,n',l}^{(j)}) \\ & \quad \times \prod_{j'=1}^J \prod_{l=1}^{M_{P,n'}^{(j,j')}} g_P(z_{P,n',l}^{(j,j')} | \mathbf{x}_{n'}, \mathbf{X}_{n'}, a_{P,n',l}^{(j,j')}) \end{aligned} \quad (15)$$

where $\Upsilon(\mathbf{x}_n | \mathbf{x}_{n-1}) \triangleq f(\mathbf{x}_n | \mathbf{x}_{n-1})$ is the state transition function. Fig. 2 is the factor graph that represents the factorization of the joint posterior in (15).

E. Problem Formulation and Solution

Our aim is to estimate the agent state \mathbf{x}_n in a sequential way based on the Bayesian framework. The agent state is estimated

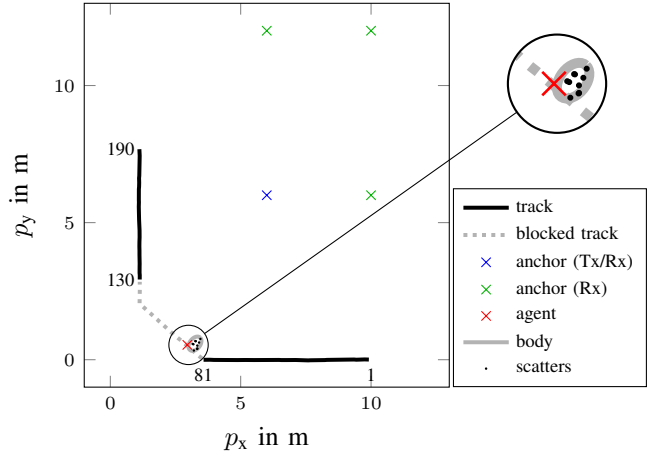


Fig. 3. Graphical representation of the synthetic trajectory and generated scatters for passive measurements. The scatters are generated with respect to one anchor at position (6, 6) for one snapshot.

by calculating the minimum mean-square error (MMSE) [34] of each time step

$$\hat{\mathbf{x}}_n^{\text{MMSE}} \triangleq \int \mathbf{x}_n f(\mathbf{x}_n | \mathbf{z}) d\mathbf{x}_n \quad (16)$$

with $\hat{\mathbf{x}}_n^{\text{MMSE}} = [\hat{\mathbf{p}}_n^{\text{MMSE T}} \hat{\mathbf{v}}_n^{\text{MMSE T}} \hat{\mathbf{b}}_n^{\text{MMSE T}}]^T$.

The state estimate in (16) is obtained by calculating the marginal posterior PDFs from the joint posterior PDFs by applying the SPA [35]. Due to the complexity of the integrals used in the SPA message calculations, analytical solutions are not feasible. As a result, we employ a particle-based representation of the message according to [25]. This approach allows us to approximately compute the required probabilities while maintaining computational efficiency.

IV. RESULTS

A. Simulation Setup

The proposed algorithm is evaluated using synthetic measurement data according to the scenario presented in Fig. 3 as well as the radio signal models put forward in Section II. The agent moves along a trajectory with two distinct direction changes. The human body, referred to as the extended object, is modeled as an ellipse with the long axis 0.3 m and short axis 0.2 m. The scatters are generated uniformly on the ellipse. The bias $[0.25, 0.1]^T$ m between the body center and the mobile agent is set to be constant among the whole trajectory. The object is observed at 190 discrete time steps at a constant observation rate of $\Delta T = 100$ ms. For active measurements, the signals are transmitted from the mobile agent and received at 4 anchors. For passive measurements, the signals are transmitted from one specific anchor at position (6, 6) and received at all considered anchors as shown in Fig. 3. We assume that the active measurements are blocked by the human body during [80, 129] time steps, which leads to full obstructed line-of-sight (OLOS) situations for part of the track. The normalized amplitudes are set to 40 dB at an LOS distance of 1 m and are assumed to follow free-space path loss, and $\beta_q = 0.2$ and $\beta_{q'} = 0.8$ are set to make sure the received scattering amplitudes are approximate by 10 dB lower

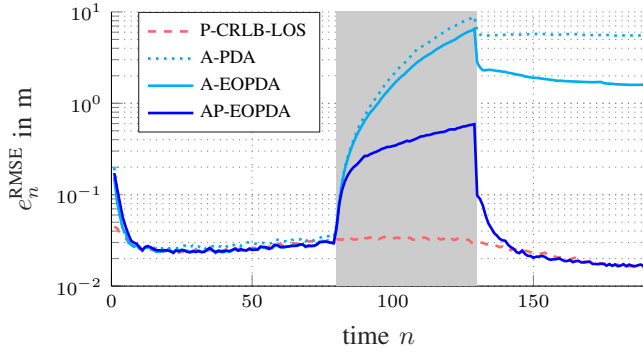


Fig. 4. RMSE of the estimated agent position based on numerical simulations.

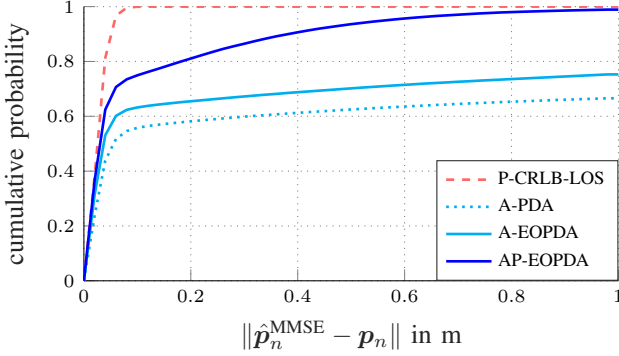


Fig. 5. The cumulative distribution of the position errors evaluated by numerical simulations over the whole time period.

than the LOS amplitude of each time step. The transmitted complex baseband signal $s(t)$ is of root-raised-cosine shape with a roll-off factor of 0.6 and a bandwidth of 500 MHz.

The agent state is represented as $\mathbf{x}_n = [\tilde{\mathbf{x}}_n^T \mathbf{b}_n^T]^T = [\mathbf{p}_n^T \mathbf{v}_n^T \mathbf{b}_n^T]^T$. The PDF of the joint agent state \mathbf{x}_n is factorized as $f(\mathbf{x}_n|\mathbf{x}_{n-1}) = f(\tilde{\mathbf{x}}_n|\tilde{\mathbf{x}}_{n-1})f(\mathbf{b}_n|\mathbf{b}_{n-1})$, where the agent motion, i.e. the state transition PDF $f(\tilde{\mathbf{x}}_n|\tilde{\mathbf{x}}_{n-1})$ is described by a linear, constant velocity and stochastic acceleration model [36, p. 273], given as $\tilde{\mathbf{x}}_n = \mathbf{A} \tilde{\mathbf{x}}_{n-1} + \mathbf{B} \mathbf{w}_n$. The acceleration process \mathbf{w}_n is i.i.d. across n , zero-mean, and Gaussian with covariance matrix $\sigma_a^2 \mathbf{I}_2$, with σ_a being the acceleration standard deviation, and $\mathbf{A} \in \mathbb{R}^{4 \times 4}$ and $\mathbf{B} \in \mathbb{R}^{4 \times 2}$ are defined according to [36, p. 273]. The state transition of the bias \mathbf{b}_n , i.e. the state transition PDF $f(\mathbf{b}_n|\mathbf{b}_{n-1})$, is $\mathbf{b}_n = \mathbf{b}_{n-1} + \varepsilon_{\mathbf{b}_n}$, where the noise $\varepsilon_{\mathbf{b}_n}$ is i.i.d. across n , zeros mean, Gaussian, with covariance matrix $\sigma_{\varepsilon_b}^2 \mathbf{I}_2$. The number of particles is set to $I = 5000$ for inference during the track, and the particles consist of all considered random variables. The state-transition variance (STV) are set as $\sigma_a = 3 \text{ m/s}^2$ and $\sigma_{\varepsilon_b} = 0.1 \text{ m}$. The other simulation parameters are as follows: the detection threshold is $\gamma = 2$ (6 dB). The mean number of object-related measurements is set to $\mu_m = 5$, and the scatters are regenerated for each time step and each anchor, for active measurements and passive measurements, respectively. The mean number of clutter is set to $\mu_c = 10$.

B. Performance Evaluation

The numerical results of active-only estimation (“A-PDA” and “A-EOPDA”) as well as joint estimation (“AP-EOPDA”)

are shown in Fig. 4 and Fig. 5, respectively. The posterior Cramér-Rao lower bound (P-CRLB) is provided as a performance baseline considering the dynamic model of the agent state [25], [37]. The “P-CRLB-LOS” is calculated by assuming the LOS component to all anchors is always available along the whole trajectory, providing a lower bound for the estimation of the object. Notably, for both active and passive simulations, we always include the scattering components in the simulated signals, but we compare the results of considering the scattering components in the active case for the data association or not. More specifically, “A-PDA” only considers one object-related measurement, the LOS component, in the PDA, while “A-EOPDA” and “AP-EOPDA” take into account multiple object-related measurements, including both the LOS component as well as scatter components. For joint estimation, we make use of scattering paths from the passive measurements, and assume the passive paths of all anchors are always available along the whole trajectory.

The results are shown in terms of the root mean squared error (RMSE) of the estimated agent position $e_n^{\text{RMSE}} = \sqrt{\mathbb{E}\{\|\hat{\mathbf{p}}_n^{\text{MMSE}} - \mathbf{p}_n\|^2\}}$, and evaluated by numerical simulation with 500 realizations. The RMSE is plotted versus the discrete measurement time n in Fig. 4. Moreover, the cumulative probability of the position errors $\|\hat{\mathbf{p}}_n^{\text{MMSE}} - \mathbf{p}_n\|$ is evaluated by numerical simulations over the whole time period and shown in Fig. 5. It can be observed that the RMSE of the joint estimation significantly outperforms the active-only estimation results during and after the full OLOS time steps. The uncertainty from the clutter becomes unacceptable for the active estimation during 50 blocked steps. This leads to outlier occurrence in the active-only results, resulting in a significant difference between the joint and active-only results after the blocked steps. Besides, comparing the estimation results of “A-PDA” and “A-EOPDA”, we can find that involving more object-related measurements reduces the number of outliers for the active estimation. Furthermore, our proposed joint estimation algorithm for the extended object, referred to as “AP-EOPDA”, achieves the “P-CRLB-LOS” exactly before the OLOS steps, and converges rapidly to the “P-CRLB-LOS” after the OLOS steps with the aid of passive measurement data. These results demonstrate that the joint estimation algorithm exhibit enhanced robustness and reliability.

V. CONCLUSION AND FUTURE WORK

The key research problem addressed in this paper is how to achieve robust and reliable positioning of a mobile agent (e.g. a mobile device carried by a person) in situations where the direct LOS between the agent and anchors is obstructed by the human body. The human body is modeled as an extended object. We developed a joint estimation method by applying the PDA for both active and passive measurements. We also consider multiple object-related measurements in the PDA for each time step. Results show that the joint estimation method achieves significantly lower RMSE during and after the OLOS steps compared to the method using only active measurements. It demonstrates that additional scattering information from passive measurements can help with the positioning during

the full OLOS case, and effectively reduce the outliers after the blocked steps. Besides, the joint estimation result attains the posterior Cramer-Rao lower bound of LOS component exactly before and after the blocked steps. The results illustrate the potential of exploiting scattering paths from the human body for robust localization when line-of-sight signals are unavailable.

According to experiments, scatter points are more prone to occur on the surface of the human body in a specific direction related to the anchors. Thus, our next step is to deal with this physics-based measurement models, and estimate the time-varying extent state together with the kinematic state. Additionally, our following research can also focus on incorporating real measurement data for the validation of the proposed "AP-EOPDA", and explore the runtime of our proposed algorithm in a realistic setup.

REFERENCES

- [1] J. Gedschold, S. Semper, R. S. Thomä, M. Döbereiner, and G. D. Galdo, "Dynamic delay-dispersive UWB-radar targets: Modeling and estimation," *IEEE Transactions on Antennas and Propagation*, vol. 71, no. 8, pp. 6814–6829, 2023.
- [2] R. Zetik, J. Sachs, and R. S. Thoma, "UWB short-range radar sensing - the architecture of a baseband, pseudo-noise UWB radar sensor," *IEEE Instrumentation & Measurement Magazine*, vol. 10, no. 2, pp. 39–45, 2007.
- [3] K. Witrisal, P. Meissner *et al.*, "High-accuracy localization for assisted living: 5G systems will turn multipath channels from foe to friend," *IEEE Signal Process. Mag.*, vol. 33, no. 2, pp. 59–70, Mar. 2016.
- [4] R. Mendrzik, H. Wymeersch, G. Bauch, and Z. Abu-Shaban, "Harnessing NLOS Components for Position and Orientation Estimation in 5G Millimeter Wave MIMO," *IEEE Trans. Wireless Commun.*, vol. 18, no. 1, pp. 93–107, 2019.
- [5] Y. Wang, K. Gu, Y. Wu, W. Dai, and Y. Shen, "NLOS effect mitigation via spatial geometry exploitation in cooperative localization," *IEEE Trans. Wireless Commun.*, vol. 19, no. 9, pp. 6037–6049, 2020.
- [6] R. Karlsson and F. Gustafsson, "The future of automotive localization algorithms: Available, reliable, and scalable localization: Anywhere and anytime," *IEEE Signal Process. Mag.*, vol. 34, no. 2, pp. 60–69, 2017.
- [7] J. Ko, T. Gao, R. Rothman, and A. Terzis, "Wireless sensing systems in clinical environments: Improving the efficiency of the patient monitoring process," *IEEE Eng. Med. Biol. Mag.*, vol. 29, pp. 103–9, 05 2010.
- [8] A. Kalyanaraman, Y. Zeng, S. Rakshit, and V. Jain, "CaraoKey : Car states sensing via the ultra-wideband keyless infrastructure," in *Proc. IEEE SECON-20*, 2020, pp. 1–9.
- [9] T. Wilding, E. Leitinger, and K. Witrisal, "Multipath-based localization and tracking considering off-body channel effects," in *2022 16th European Conference on Antennas and Propagation (EuCAP)*, 2022, pp. 1–5.
- [10] J. W. Koch, "Bayesian approach to extended object and cluster tracking using random matrices," *IEEE Transactions on Aerospace and Electronic Systems*, vol. 44, no. 3, pp. 1042–1059, 2008.
- [11] M. Feldmann and D. Franken, "Tracking of extended objects and group targets using random matrices – a new approach," in *2008 11th International Conference on Information Fusion*, 2008, pp. 1–8.
- [12] M. Feldmann, D. Fränken, and W. Koch, "Tracking of extended objects and group targets using random matrices," *IEEE Transactions on Signal Processing*, vol. 59, no. 4, pp. 1409–1420, 2011.
- [13] M. Schuster, J. Reuter, and G. Wanielik, "Probabilistic data association for tracking extended targets under clutter using random matrices," in *2015 18th International Conference on Information Fusion (Fusion)*, 2015, pp. 961–968.
- [14] L. Zhang and J. Lan, "Tracking of extended object using random matrix with non-uniformly distributed measurements," *IEEE Transactions on Signal Processing*, vol. 69, pp. 3812–3825, 2021.
- [15] K. Granström, S. Reuter, D. Meissner, and A. Scheel, "A multiple model PHD approach to tracking of cars under an assumed rectangular shape," in *17th International Conference on Information Fusion (FUSION)*, 2014, pp. 1–8.
- [16] K. Granström, C. Lundquist, and U. Orguner, "Tracking rectangular and elliptical extended targets using laser measurements," in *14th International Conference on Information Fusion*, 2011, pp. 1–8.
- [17] M. Baum and U. D. Hanebeck, "Extended object tracking with random hypersurface models," *IEEE Transactions on Aerospace and Electronic Systems*, vol. 50, no. 1, pp. 149–159, 2014.
- [18] T. Hirscher, A. Scheel, S. Reuter, and K. Dietmayer, "Multiple extended object tracking using gaussian processes," in *2016 19th International Conference on Information Fusion (FUSION)*, 2016, pp. 868–875.
- [19] M. Kumru and E. Özkan, "Three-dimensional extended object tracking and shape learning using gaussian processes," *IEEE Transactions on Aerospace and Electronic Systems*, vol. 57, no. 5, pp. 2795–2814, 2021.
- [20] F. Meyer, Z. Liu, and M. Z. Win, "Scalable probabilistic data association with extended objects," in *2019 IEEE International Conference on Communications Workshops (ICC Workshops)*, 2019, pp. 1–6.
- [21] F. Meyer and J. L. Williams, "Scalable detection and tracking of geometric extended objects," *IEEE Transactions on Signal Processing*, vol. 69, pp. 6283–6298, 2021.
- [22] L. Wielandner, A. Venus, T. Wilding, and E. Leitinger, "Multipath-based SLAM for non-ideal reflective surfaces exploiting multiple-measurement data association," *accepted in Journal of Advances in Information Fusion*, 2023. [Online]. Available: <http://arxiv.org/abs/2304.05680>
- [23] Y. Bar-Shalom, F. Daum, and J. Huang, "The probabilistic data association filter," *IEEE Control Syst. Mag.*, vol. 29, no. 6, pp. 82–100, Dec 2009.
- [24] E. Leitinger, A. Venus, B. Teague, and F. Meyer, "Data fusion for multipath-based SLAM: Combining information from multiple propagation paths," *IEEE Trans. Signal Process.*, 2023.
- [25] A. Venus, S. Tertinek, and K. Witrisal, "A graph-based algorithm for robust sequential localization exploiting multipath for obstructed-LOS-bias mitigation," *IEEE Trans. Wireless Commun.*, 2023.
- [26] A. Venus, E. Leitinger, S. Tertinek, F. Meyer, and K. Witrisal, "Graph-based simultaneous localization and bias tracking," *ArXiv e-prints*, 2023. [Online]. Available: <http://arxiv.org/abs/2310.02814>
- [27] F. M. Schubert, M. L. Jakobsen, and B. H. Fleury, "Non-stationary propagation model for scattering volumes with an application to the rural LMS channel," *IEEE Transactions on Antennas and Propagation*, vol. 61, no. 5, pp. 2817–2828, 2013.
- [28] T. Wilding, E. Leitinger, U. Muehlmann, and K. Witrisal, "Modeling human body influence in UWB channels," in *2020 IEEE 31st Annual International Symposium on Personal, Indoor and Mobile Radio Communications*, 2020, pp. 1–6.
- [29] P. Hoher, S. Wirtensohn, T. Baur, J. Reuter, F. Govaers, and W. Koch, "Extended target tracking with a lidar sensor using random matrices and a virtual measurement model," *IEEE Transactions on Signal Processing*, vol. 70, pp. 228–239, 2022.
- [30] K. Witrisal, E. Leitinger, S. Hinteregger, and P. Meissner, "Bandwidth scaling and diversity gain for ranging and positioning in dense multipath channels," *IEEE Wireless Commun. Lett.*, vol. 5, no. 4, pp. 396–399, Aug. 2016.
- [31] E. Leitinger, P. Meissner, C. Ruedisser, G. Dumphart, and K. Witrisal, "Evaluation of position-related information in multipath components for indoor positioning," *IEEE J. Sel. Areas Commun.*, vol. 33, no. 11, pp. 2313–2328, Nov. 2015.
- [32] E. Wan and R. Van Der Merwe, "The unscented kalman filter for non-linear estimation," in *Proceedings of the IEEE 2000 Adaptive Systems for Signal Processing, Communications, and Control Symposium (Cat. No.00EX373)*, 2000, pp. 153–158.
- [33] F. Meyer, T. Kropfreiter, J. L. Williams, R. Lau, F. Hlawatsch, P. Braca, and M. Z. Win, "Message passing algorithms for scalable multitarget tracking," *Proc. IEEE*, vol. 106, no. 2, pp. 221–259, Feb. 2018.
- [34] S. Kay, *Fundamentals of Statistical Signal Processing: Estimation Theory*. Upper Saddle River, NJ, USA: Prentice Hall, 1993.
- [35] F. Kschischang, B. Frey, and H.-A. Loeliger, "Factor graphs and the sum-product algorithm," *IEEE Trans. Inf. Theory*, vol. 47, no. 2, pp. 498–519, Feb. 2001.
- [36] Y. Bar-Shalom, T. Kirubarajan, and X.-R. Li, *Estimation with Applications to Tracking and Navigation*. New York, NY, USA: John Wiley & Sons, Inc., 2002.
- [37] P. Tichavsky, C. Muravchik, and A. Nehorai, "Posterior Cramer-Rao bounds for discrete-time nonlinear filtering," *IEEE Trans. Signal Process.*, vol. 46, no. 5, pp. 1386–1396, May 1998.